Evolution of structural and magnetic properties in $Ta/Ni_{81}Fe_{19}$ multilayer thin films

I. Hashim and H. A. Atwater
Thomas J. Watson Laboratory of Applied Physics, California Institute of Technology, Pasadena, California 91125

K. T. Y. Kung and R. M. Valletta
IBM Almaden Research Center, San Jose, California 95120

(Received 27 October 1992; accepted for publication 5 March 1993)

The interdiffusion kinetics in short period (12.8 nm) $Ta/Ni_{81}Fe_{19}$ polycrystalline multilayer films has been investigated and related to the evolution of soft magnetic properties upon thermal annealing in the temperature range 300–600 °C. Small angle x-ray diffraction and transmission electron microscopy were used to estimate the multilayer period. Interdiffusion in the multilayers was directly computed from the decay of the satellites near (000) in a small angle x-ray diffraction spectrum. A kinetic analysis of interdiffusion suggests that grain growth is concurrent with grain boundary diffusion of Ta in $Ni_{81}Fe_{19}$. The evolution of soft magnetic properties of $Ni_{81}Fe_{19}$, i.e., lowering of $4\pi M_s$ and increase in coercivity H_c, also lend support to the above analysis.

I. INTRODUCTION

A. Motivation

Thin films of $Ni_{81}Fe_{19}$ (Permalloy) are of considerable interest to magnetoresistive sensors owing to their favorable soft magnetic properties such as low magnetocrystalline anisotropy, low magnetostriction, and high permeability. Moreover, recent developments of soft magnetic multilayer films whose layer thickness are small enough to permit coupling between magnetic layers have the potential to result in magnetic sensors with much higher magnetoresistance than that observed in single layer films.[1,2] However, these properties depend sensitively on the microstructure of the film which is related to the film deposition conditions, as well as post-growth thermal annealing. The objective of this paper is to relate the evolution of microstructure to soft magnetic properties during thermal annealing of multilayer films which are composed of sequences of $Ni_{81}Fe_{19}/Ta$ bilayers.

The resistivity and magnetoresistance of polycrystalline $Ni_{81}Fe_{19}$ films are affected by grain boundary and interfacial scattering,[3] so achievement of larger grain sizes compared to the mean free path for electron scattering is desirable. One approach to reducing grain boundary scattering is by thermally induced grain growth. For $Ni_{81}Fe_{19}$ thin films, two activation energies for grain growth have been estimated from changes in resistivity with thermal annealing; they are 0.70 ± 0.05 and 1.86 ± 0.15 eV, accounting for grain growth in two temperature regimes.[4] However, annealing treatments have been reported to adversely affect the soft magnetic properties of $Ni_{81}Fe_{19}$; in particular, the coercivity H_c increases.[5] A possible cause for the increase in coercivity is the phenomenon of thermal grooving which occurs at grain boundaries in polycrystalline film. During thermal annealing, grain boundary grooves deepen and eventually lead to the formation of voids between grains,[6] and the transport of matter away from the grooves often takes place via surface diffusion. However, if the polycrystalline film is encapsulated, groove formation may be significantly retarded, presumably due to inhibition of surface diffusion.[7]

In multilayer films, interdiffusion into $Ni_{81}Fe_{19}$ layers from adjacent films during annealing can dramatically affect its magnetic properties. The thermal stability of $Ti/Ni_{81}Fe_{19}$ films has been investigated using diffusion couples and high-angle x-ray diffraction.[8] However, quantitative conclusions about kinetics of interdiffusion could not be obtained from that study because of insensitivity of the characterization method used. In this paper, we present a detailed analysis of interdiffusion kinetics of $Ta/Ni_{81}Fe_{19}$ using small angle x-ray diffraction (SAXD) from multilayers, which is an extremely sensitive probe of interdiffusion at low temperatures.[9] Ta is typically used as an encapsulation material for $Ni_{81}Fe_{19}$ films in magnetoresistive sensors, and has been investigated as the nonmagnetic component layer in multilayer films.[10] The Ni-Ta phase diagram indicates relatively high Ta solubility in Ni (7 at. % at 600 °C),[11] whereas solubility of Ni in Ta is much lower (<0.14 at. % at 600 °C). Thus, Ta diffusion into $Ni_{81}Fe_{19}$ is anticipated upon annealing at sufficiently high temperatures. The presence of Ta in Ni is known to lead to a reduction in magnetic moment (20 at. % Ta in Ni reduces its magnetic moment to zero[12]). This suggests that the $Ta/Ni_{81}Fe_{19}$ system can be used to investigate very quantitative correlations between interdiffusion and changes in soft magnetic properties of $Ni_{81}Fe_{19}$. Finally, SAXD has not been used as commonly for detailed analysis of interdiffusion in polycrystalline films as for amorphous or epitaxial films.[9] In view of that, we present here a model to enable the application of SAXD to analyze grain-boundary diffusion with concurrent grain growth in polycrystalline multilayers.

 0021-8979/93/74(1)/458/7/$6.00

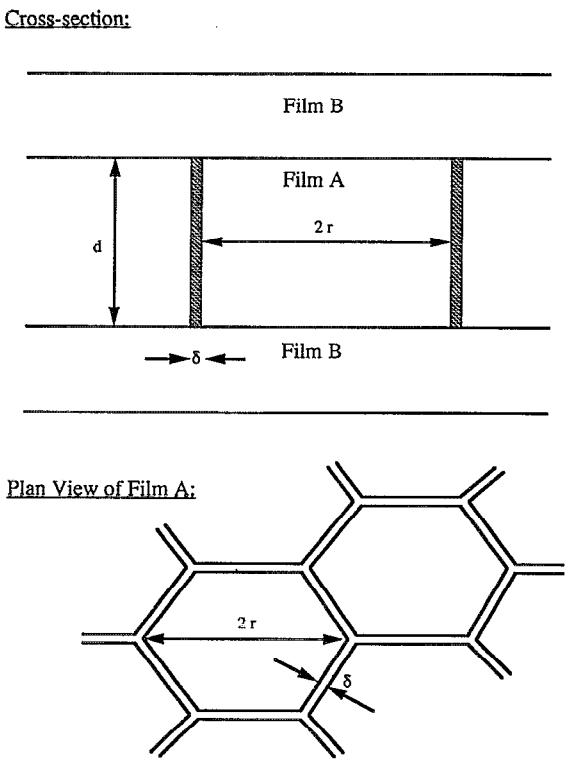

FIG. 1. Model for grain-boundary diffusion in a columnar-grained thin film shown in (a) cross section and (b) plan view.

II. CONCURRENT GRAIN GROWTH AND GRAIN-BOUNDARY DIFFUSION

A standard analysis for interdiffusion in multilayers[9] predicts a constant logarithmic decay of mth satellite intensity, I_m, given by

$$\frac{\partial \ln I_m}{\partial t} = -\frac{8\pi^2 m^2}{d^2} D, \tag{1}$$

where d is the multilayer period and D is the diffusion constant for the multilayer. In short period multilayer films, the appropriate diffusion constant D is, in principle, not equal to the bulk diffusion constant for dilute solutions. However, as indicated in Appendix A, this is not an unreasonable assumption in the present analysis. Equation (1) is appropriate when diffusion mechanism occurs in a bulk manner as in lattice diffusion. However, in polycrystalline films, grain-boundary diffusion is generally the dominant diffusion mechanism at lower temperatures. Consider a thin film of composition A with a columnar-grained microstructure, which is modeled for simplicity as an array of close-packed hexagons so that the hexagon extremal cross section is twice the grain radius r and height equal to film thickness d, as shown in Fig. 1. If the grain-boundary width is δ, and the film of composition A has interfaces to films of composition B on top and bottom, then the grain-boundary area in the plane of the film per grain, defined as the grain-boundary density, to first order is $6r\delta/3r^2$. If temperature is low enough such that lattice diffusion is negligible compared to grain-boundary diffusion, then the appropriate diffusion constant D of Eq. (1) is the grain-boundary diffusion constant D_{gb}, weighted by the grain-boundary density:

$$D = D_{gb}\frac{2\delta}{r}. \tag{2}$$

However, the analysis is further complicated by the possibility of concurrent grain growth which decreases the grain boundary density. Grain growth kinetics in thin films typically obey the semiempirical relationship:[13]

$$r^n(t) - r^n(0) = \alpha e^{-Q_{gbm}/kT} t \equiv A(T)t, \tag{3}$$

where $r(t)$ is the mean grain size at time t, $r(0)$ is the initial mean grain size, α is a weakly temperature-dependent constant, n is typically in the range of 2–4, and Q_{gbm} is the activation energy for grain boundary migration. The kinetic models for grain growth typically imply value of 2 for the exponent n. However, in thin films, grain growth is typically saturated, i.e., undergoes a rapid reduction in growth rate as the grain size approaches the layer thickness.[13] As a consequence, the experimental data fits better to an exponent in the range of $n=3$–4 at later times. Assuming that the grain-boundary density decreases due to grain growth as given by Eq. (3), the appropriate diffusion equation for this problem is

$$\frac{[r^n(0)+A(T)t]^{1/n}}{2\delta}\frac{\partial C(z,t)}{\partial t} = D_{gb}\frac{\partial^2 C(z,t)}{\partial z^2}, \tag{4}$$

where $C(z,t)$ is the concentration of the multilayer. Equation (4) can be solved using separation of variables and Fourier decomposition in spatial variable z, analogously to the ordinary diffusion equation. The solution can be written as

$$C(z,t) = \sum_{m=0}^{\infty} A_m \exp\left[-\left(\frac{n}{n-1}\right)k_m^2 \frac{2D_{gb}\delta}{A(T)} \times [r^n(0)+A(T)t]^{1-(1/n)}\right]\cos(k_m z+\phi_m). \tag{5}$$

Since the electron density $\rho_e(z,t)$ of the multilayer varies linearly with $C(z,t)$, and the intensity of the mth satellite $I_m(t)$ in SAXD spectrum goes as square of the mth Fourier component of $\rho_e(z,t)$, the time dependence of I_m will be given by

$$I_m(t) \propto \exp\left[-2k_m^2 \frac{n}{n-1}\frac{2D_{gb}\delta}{A(T)} \times [r^n(0)+A(T)t]^{1-(1/n)}\right]. \tag{6}$$

Hence, the rate of decay of $\log I_m(t)$ becomes

$$\frac{\partial \ln I_m}{\partial t} = -\frac{16\pi^2 m^2}{d^2}\frac{D_{gb}\delta}{r(t)}. \tag{7}$$

Comparing Eq. (7) with Eq. (1), note that D has been replaced by $2D_{gb}\delta/r(t)$ which is a time-dependent diffusion constant.

III. EXPERIMENTAL PROCEDURES

Multilayers composed of 15 periods of alternating layers of Ta and $Ni_{81}Fe_{19}$ were deposited on borosilicate glass and SiO_2/Si substrates using Ar^+ ion beam sputtering. The ion beam diameter at the source was 2.5 cm. The multilayers were deposited after achieving a base pressure of 5×10^{-10} Torr; Ar pressure during deposition was about 2×10^{-4} Torr. Both targets ($Ni_{81}Fe_{19}$ and Ta) were sputter etched approximately 500 Å prior to deposition. The film thickness during deposition was monitored using a calibrated crystal-oscillator thickness monitor and the deposition rate was approximately 1 Å/s. The substrate was rotated during deposition to improve film thickness uniformity. The film thickness uniformity of 300 Å $Ni_{81}Fe_{19}$ films deposited in this chamber was measured to be 2%–4%, using an optical thickness measurement apparatus. A permanent magnet was placed below the substrate during deposition to induce a uniaxial magnetic anisotropy in the $Ni_{81}Fe_{19}$ films. All post-growth anneals were carried out in a vacuum annealing furnace after achieving a base pressure of 1×10^{-16} Torr.

For SAXD, a θ–2θ x-ray diffractometer with a Cu K_α tube was employed; the sample holder was mounted on high-resolution rotation and translation stages, allowing accurate alignment of the sample with respect to the main beam. Figure 2(a) shows SAXD scan of as-deposited multilayer (period $d=128$ Å) using Cu K_α x-ray radiation. High angle x-ray diffraction spectra were obtained on another thin film x-ray diffractometer, equipped with a Mo K_α tube (see Fig. 3). Transmission electron microscopy was performed at 300 kV. Magnetic characterization was done on a 10 Hz magnetic hysteresis loop apparatus and the measured magnetic properties included coercivity H_c, magnetic anisotropy H_k, saturation and remanent magnetizations (B_s and B_r) for both easy and hard axes.

IV. STRUCTURAL CHARACTERIZATION

The characterization of an as-deposited multilayer was done from SAXD scan shown in Fig. 2(a); the characteristic oscillations superposed on the third satellite are probably due to an aperiodicity in multilayer which can be observed in cross-sectional transmission electron microscope (XTEM) images of the multilayer. Nevertheless, higher satellites can be identified easily from the SAXD spectrum. The position of these higher satellites are obtained by modeling the refractive indices n_a and n_b for individual layers in a bilayered periodic multilayer, as

$$n=1-\delta-i\beta, \tag{8}$$

where δ and β represent the multiple scattering and absorption of the x rays in matter.[14,15] Typically, δ, $\beta\ll1$ and furthermore, β is an order of magnitude smaller than δ; hence, it will be neglected in subsequent analysis. The condition for diffraction for x ray of wavelength λ in such a bilayered periodic multilayer of period $d=d_a+d_b$ becomes

$$m\lambda=2n_ad_a\sin\theta_a+2n_bd_b\sin\theta_b. \tag{9}$$

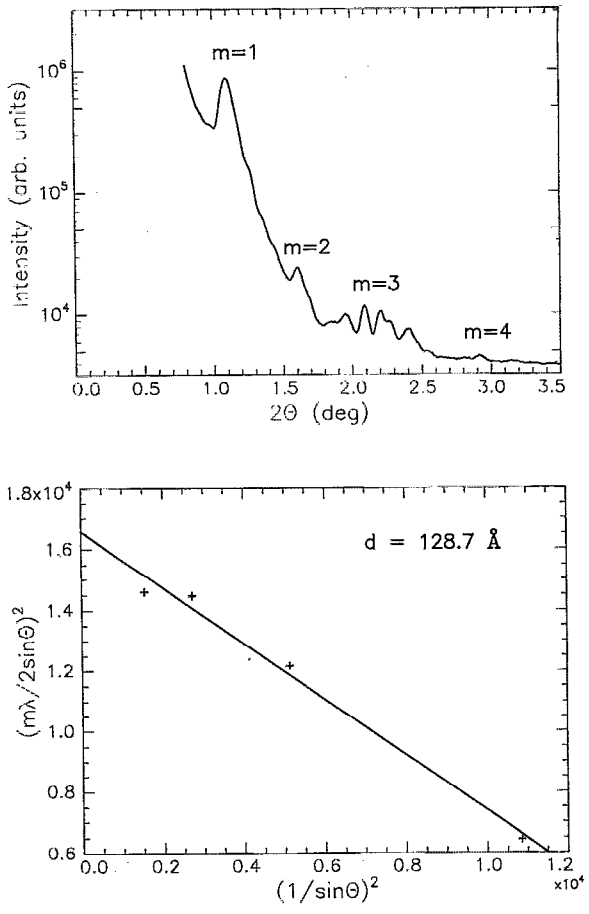

FIG. 2. (a) Small angle x-ray reflectivity of as-deposited Ta/$Ni_{81}Fe_{19}$ multilayer (15×128 Å) using Cu K_α radiation. (b) Characterization of as-deposited multilayer period from satellites observed in small angle x-ray spectrum.

Since the difference in δ for the individual layers is small, $\theta_a\approx\theta_b$. As a result, Bragg's law, modified for periodic multilayer, can be written as

$$\left(\frac{m\lambda}{2\sin\theta}\right)^2=d^2\left(1-\frac{2\langle\delta\rangle}{\sin^2\theta}\right), \tag{10}$$

where $\langle\delta\rangle$ represents a weighted average of the real part of the x-ray refractive index in the multilayer.[14] By doing a linear fit as shown in Fig. 2(b), to $(m\lambda/2\sin\theta)^2$ vs $1/\sin^2\theta$ for these satellites, the multilayer period d was found to be 128.7±21.3 Å. A fit to the SAXD spectrum was done using optical multilayer simulations.[14] The ratio of satellite peak intensities was used to calculate the average thickness of $Ni_{81}Fe_{19}$ and Ta layers, which were found to be 84±12 and 45±9 Å, respectively. Cross-sectional transmission electron micrsoscopy of multilayers, as shown in bright field in Fig. 4(a), gave period and layer thicknesses of $Ni_{81}Fe_{19}$ and Ta in excellent agreement with x-ray characterization.

As can be observed from the broader peaks due to Ta, in the x-ray diffraction pattern [see Fig. 3(a)], Ta has a much smaller grain size than $Ni_{81}Fe_{19}$; nevertheless, it is not amorphous as is indicated by the presence of many higher order peaks of *bcc* Ta. To resolve this issue further,

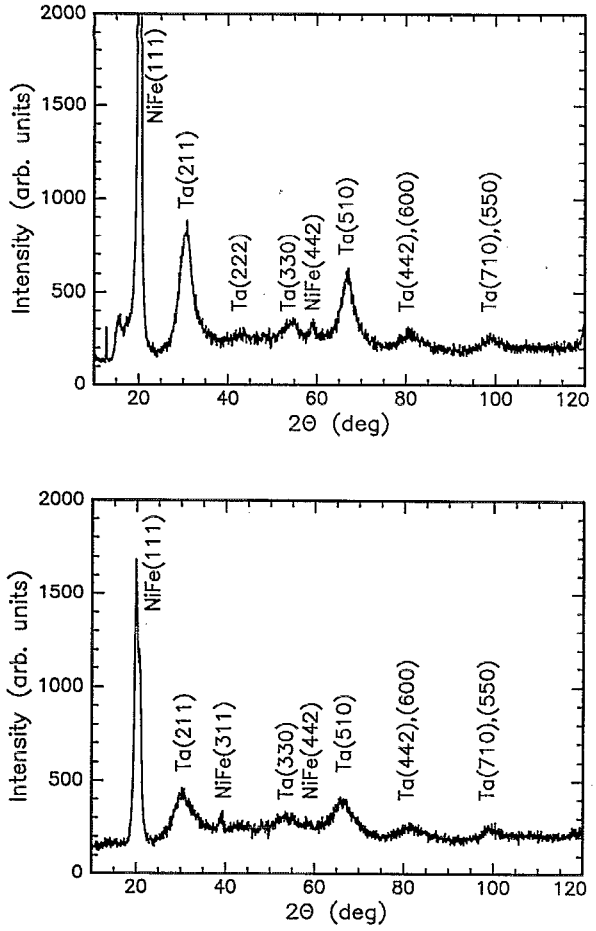

FIG. 3. (a) High angle x-ray diffraction spectra using Mo K_α radiation of as-deposited Ta/$Ni_{81}Fe_{19}$ multilayer and (b) after annealing at 525 °C for 4 h.

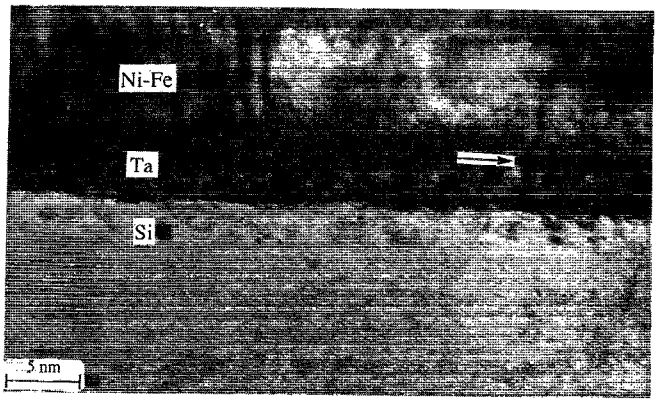

FIG. 5. High resolution cross-sectional transmission electron micrograph of $Ni_{81}Fe_{19}$/Ta multilayer as deposited on Si(111).

high-resolution imaging of multilayers deposited on Si(111) was done using XTEM. Si was chosen as a substrate since it is difficult to do high resolution imaging of polycrystalline metal films on glass. As can be seen in Fig. 5, parts of the silicon substrate and possibly Ta film as well, have been amorphized by ion milling. However, columnar grains extending from Ta film to $Ni_{81}Fe_{19}$ can still be distinguished towards the right of the micrograph, as indicated by an arrow in Fig. 5. Using XTEM images and high angle x-ray diffraction spectra of as-deposited multilayers, an average grain size of 60 and 20 Å was estimated for $Ni_{81}Fe_{19}$ and Ta films, respectively. From other investigations of grain growth in $Ni_{81}Fe_{19}$ films,[16] the grain size was found to scale with film thickness and depend on growth conditions.

V. INTERDIFFUSION KINETICS

Small angle x-ray diffraction was used to study interdiffusion in multilayers which were annealed at various temperatures in the range 300–600 °C. As the decay rate of the log of satellite intensity is proportional to m^2, as given by Eq. (1), the higher satellites are more sensitive to interdiffusion at lower temperatures. The decay of higher satellites for short period multilayers can be used to measure interdiffusion lengths of a few angstroms. Figure 6(a) shows the integrated first satellite intensity versus cumulative annealing time at various temperatures. No change in any of the satellite intensities was observed at 300 °C. As shown in Fig. 6(a), there was no significant change in the first satellite intensity, also at 375 °C. However, we were able to characterize interdiffusion at this temperature from the decay of the higher order satellites [see Fig. 6(b)]. As it can be seen from Fig. 6, the satellite intensities do not have a constant decay rate as predicted by analysis of Ref. 9. A better fit to the data, superposed as dashed lines in Fig. 6(a), was obtained using the model described above

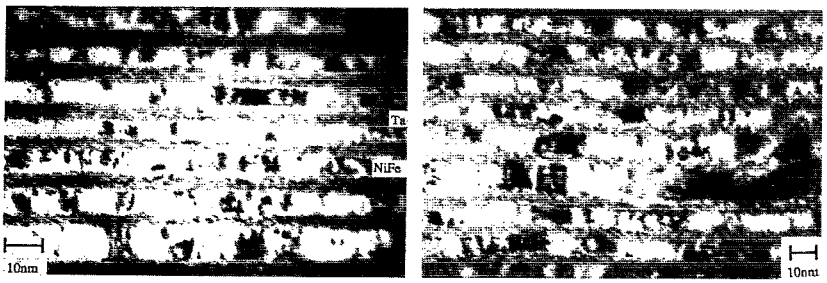

FIG. 4. (a) Bright field cross-sectional transmission electron micrograph of as-deposited multilayer (15×128 Å) and (b) after annealing at 525 °C for 4 h.

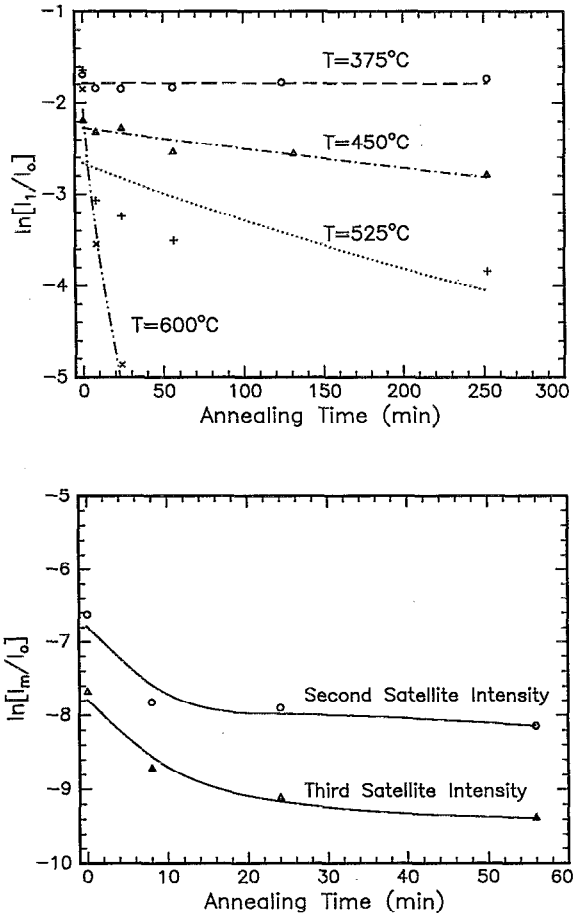

FIG. 6. (a) Variation of first satellite intensity with cumulative annealing time at various temperatures and fit to decay of satellite intensities using model for concurrent grain growth and grain-boundary diffusion. (b) Second and third satellite intensities vs cumulative annealing time at 375 °C.

for concurrent grain growth and grain boundary diffusion. Quantative analysis of grain growth in polycrystalline multilayer films is complicated by the superposition of the microstructure of the individual layers when imaged in plan view or cross-section electron microscopy. As a result, evidence for grain growth in the temperature range 300–600 °C was also obtained from investigation of single layer $Ni_{81}Fe_{19}$ thin films which were annealed in high vacuum and analyzed by plan view TEM. The mean grain size in these studies was calculated by averaging over up to 100 grains contained in bright field TEM micrographs. Although this type of grain growth analysis is not as desirable as analysis of the multilayers themselves, the results for grain growth in single layer films are qualitatively consistent with observations of increased grain size in the thin regions of multilayer cross sections. The evolution of transport properties and microstructure of single layer $Ni_{81}Fe_{19}$ films will be reported elsewhere.[16]

Assuming parabolic grain growth kinetics ($n=2$), Eq. (6) becomes

$$\ln\frac{I_m(t)}{I_0}=-\frac{16\pi^2m^2}{d^2}\,D\frac{r^2(0)}{A(T)}\left[1+\frac{A(T)t}{r^2(0)}\right]^{1/2}, \qquad (11)$$

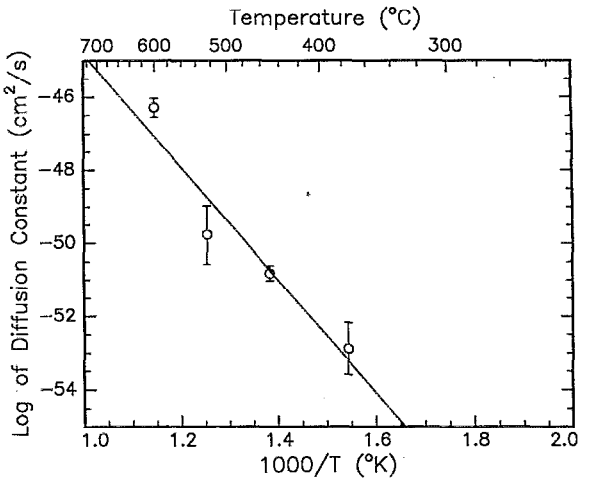

FIG. 7. Arrhenius plot of D with temperature to estimate activation energy and preexponential for interdiffusion.

where I_0 is the constant of integration chosen so that $I_m(t=0)$ computed from above equation matches experimentally observed mth satellite intensity at $t=0$. Using Eq. (11), a fit was done to decay of observed satellite intensities, as shown in Fig. 6(a), to calculate D. The initial grain size $r(0)$ and α were calculated from grain growth analysis of single layer $Ni_{81}Fe_{19}$ films[16] and found to be 60.37 Å and 5.24×10^{-15} cm^2/s, respectively. Based on this analysis, the activation energy for grain boundary migration, Q_{gbm}, for single layer $Ni_{81}Fe_{19}$ films was found to be 0.55 ± 0.11 eV. An Arrhenius plot of D, shown in Fig. 7, yielded the following diffusion coefficient and activation energy:

$$D_0=1.70\times10^{-9}\ \text{cm}^2/\text{s}, \quad Q=1.28\pm0.26\ \text{eV}.$$

No information on Ta lattice diffusion in $Ni_{81}Fe_{19}$ or vice versa was available. However, following diffusion constants for lattice self-diffusion in Ni[17] and Ta[18] are known from previous studies:

Ni: $D_0=1.30$ cm^2/s, $Q_l=2.27$ eV,

Ta: $D_0=0.124$ cm^2/s, $Q_l=4.2$ eV.

Typically, the activation energy for grain boundary diffusion is significantly less than that for lattice diffusion ($Q_{gb}\approx0.4$–$0.7Q_l$ for most metals[19]). Comparing activation energies for lattice diffusion to the experimentally observed activation energy agrees with our assumption that the interdiffusion mechanism is grain-boundary diffusion. The relatively small value of preexponential found experimentally can be explained by the fact that D has been weighted by the grain-boundary density.

High angle x-ray diffraction spectra of as-deposited and annealed multilayers, shown in Fig. 3, indicate that the *bcc* Ta crystalline peaks were broadened after a 4 h anneal at 525 °C, which might suggest a diminishing crystal size due to grain boundary mediated solid-state amorphization. However, the persistence of *bcc* Ta crystalline peaks in the x-ray spectrum and the polycrystalline nature of the $Ni_{81}Fe_{19}$ film, as evidenced by the micrograph of Fig. 4,

suggest that a solid-state amorphization reaction may have begun but has not resulted in transformation of a significant fraction of the Ta film. In this temperature regime, a solid-state amorphization reaction between Ni and β-Ta multilayers was reported by Hollanders *et al.*[20] for multilayer films. Solid-state amorphization typically precedes nucleation of a crystalline intermetallic compound phase[21] whose presence was not observed in high angle x-ray diffraction spectra after prolonged anneals up to 525 °C.

Comparison of the bright field micrographs of an as-deposited multilayer and another after annealing at 525 °C for 4 h, as shown in Fig. 4, indicates that the $Ni_{81}Fe_{19}$-Ta interface is roughened and more diffuse after annealing at 525 °C. No quantitative information about the diffusion constants for the different constituents could be obtained from the above analysis. However, evolution of magnetic properties, as discussed below, indicates that there is accumulation of Ta at $Ni_{81}Fe_{19}$ grain boundaries. This is consistent with our diffusion kinetics analysis which suggests grain-boundary diffusion as the mechanism for interdiffusion. The enhanced contrast at $Ni_{81}Fe_{19}$ grain boundaries in the bright field micrographs of multilayer annealed at 525 °C, suggests that $Ni_{81}Fe_{19}$ grain boundaries are Ta rich. However, as the magnetic properties of the multilayer are not as sensitive to outdiffusion of Ni and Fe into Ta, that possibility cannot be ruled out.

VI. EVOLUTION OF MAGNETIC PROPERTIES

B-H loop measurements were made for the as-deposited Ta/$Ni_{81}Fe_{19}$ multilayer after thermal annealing at 300, 375, 450, and 525 °C for 4 h. The coercivity of the as-deposited multilayer was 0.5 Oe, and increased to 6.5 Oe after annealing at 525 °C. The coercivity is plotted vs interdiffusion length, which is calculated directly from the decay of the first satellite with annealing, in Fig. 8(a). The $4\pi M_s$ measurement of the as-deposited multilayer indicated an average magnetic thickness of 53.9 Å/period implying that 30.1 Å/period was nonmagnetic. This suggests the presence of 15 Å thick nonmagnetic $Ni_{81}Fe_{19}$ at each interface of $Ni_{81}Fe_{19}$ with Ta. The *B-H* loops for the as-deposited multilayer were found to be isotropic, so H_k could not be measured. However, single layer $Ni_{81}Fe_{19}$ films with thicknesses equal to or greater than 100 Å, under the same deposition conditions, were found to have well-defined easy and hard axes. The disappearance of induced uniaxial anisotropy for ultrathin $Ni_{81}Fe_{19}$ films has also been reported elsewhere.[22]

After annealing at 300 °C, the change in $4\pi M_s$ of the multilayer was less than 0.5%. This is consistent with the interdiffusion data, as no change in satellite intensities was observed at 300 °C. At higher temperatures, $4\pi M_s$ dropped sharply, as shown in Fig. 8(b). For multilayers annealed at 450 °C and higher temperatures, the field required to saturate the magnetization increased dramatically. A field greater than 100 Oe was required to saturate the multilayer annealed at 525 °C. This is also illustrated by the variation of B_r/B_s with interdiffusion length in Fig. 8(c). The transition from soft to hard magnetic properties can also be understood in terms of our analysis of interdiffusion data, if

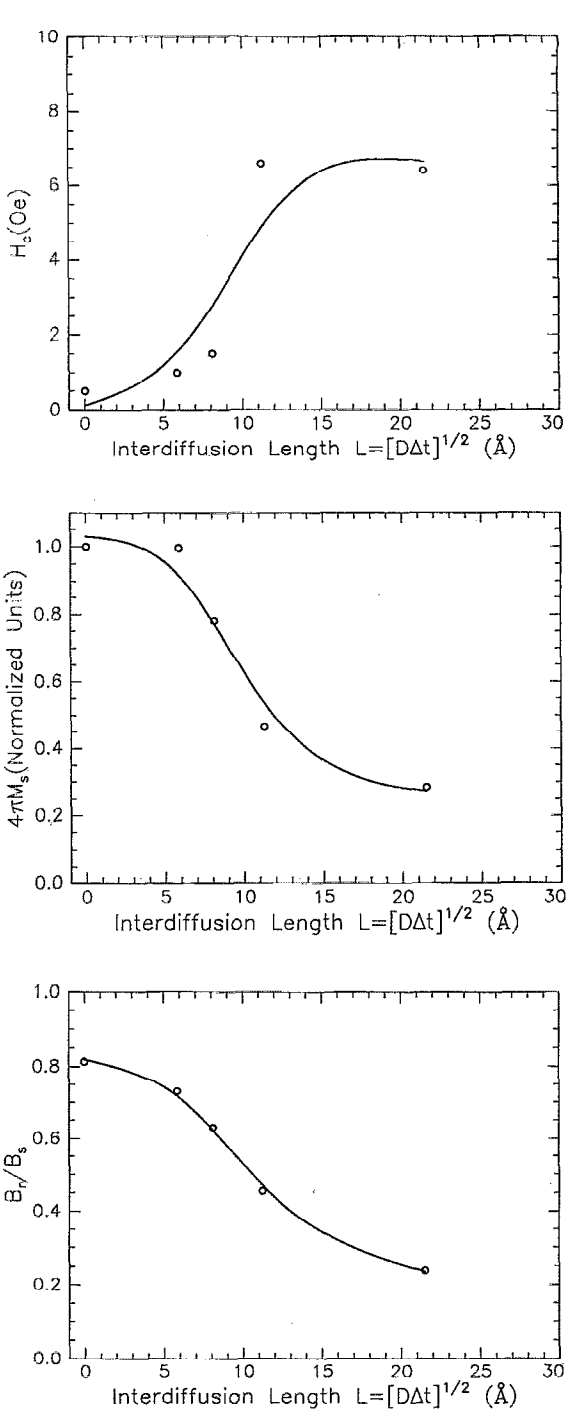

FIG. 8. Variation of (a) H_c, (b) normalized $4\pi M_s$, and (c) B_r/B_s for Ta/$Ni_{81}Fe_{19}$ multilayer with interdiffusion lengths corresponding to 4 h anneals at 300, 375, 450, and 525 °C. The solid lines are guides to the eye.

it is assumed that accumulation of Ta at $Ni_{81}Fe_{19}$ grain boundaries results in a microstructure consisting of ferromagnetic $Ni_{81}Fe_{19}$ particles embedded in a nonmagnetic Ta-$Ni_{81}Fe_{19}$ matrix. As the thickness of this nonmagnetic matrix increases, the coupling between the magnetic particles decreases, thus requiring higher saturating fields. Thus the magnetic microstructure evolves from soft, magnetically continuous layers of $Ni_{81}Fe_{19}$ to isolated $Ni_{81}Fe_{19}$ nanometer-scale particles. It is interesting to note that sim-

ilar *B-H* loop characteristics have been reported in work on a photolithographically defined array of micron-sized $Ni_{81}Fe_{19}$ particles as the interparticle spacing increases,[23] although it should be pointed out that the magnetic length scales in these two experiments are quite different. In any case, the present work suggests that evolution of film microstructure can be used to modify magnetic properties at the scale of the grain size in $Ni_{81}Fe_{19}$ films.

VII. CONCLUSIONS

Using small angle x-ray diffraction, interdiffusion lengths ranging from 5 to 40 Å were measured for Ta/$Ni_{81}Fe_{19}$ multilayers in the temperature range 300–600 °C. Thermodynamic information and TEM analysis suggests that Ta diffusion into $Ni_{81}Fe_{19}$ can occur. The interdiffusion kinetics are consistent with grain boundary diffusion of Ta concurrent with grain growth in $Ni_{81}Fe_{19}$. The evolution of soft magnetic properties of the multilayer with annealing was consistent with changes observed in its microstructure. Significantly, the change in saturation magnetization of the Ta/$Ni_{81}Fe_{19}$ multilayer upon annealing at 300 °C for 4 h was less than 0.5%. However, at temperatures higher than 375 °C, $4\pi M_s$ decreased dramatically due to interdiffusion of Ta in $Ni_{81}Fe_{19}$. Grain-boundary diffusion of Ta into $Ni_{81}Fe_{19}$ led to a microstructure consisting of isolated $Ni_{81}Fe_{19}$ particles embedded in a nonmagnetic matrix, thus increasing the field required to saturate the multilayer.

ACKNOWLEDGMENTS

This work was supported by IBM and the National Science Foundation. Diffraction analysis performed at Caltech was made possible by DOE Grant DE-FG0589ER75511. We thank C. M. Garland for assistance with electron microscopy.

APPENDIX: DIFFUSION CONSTANT FOR PERIODIC MULTILAYERS

Analysis leading to Eq. (1) assumes Fickian diffusion which does not include contributions to free energy from the concentration gradients at the interface. If the period of the multilayer is small enough,[24] the diffusion constant for the multilayer may not necessarily be the same as the bulk diffusion constant. When gradient energy contributions are important, it is wavelength dependent as given by [24]

$$D_{\lambda,m}=D\left(1+\frac{2\kappa}{f''}k_m^2\right), \tag{A1}$$

where κ is the gradient energy coefficient, f'' is the second spatial derivative of the free energy per unit volume, and D is the bulk diffusion constant. Both κ and f'' can be estimated using the regular solution model.[24] Using the heat of mixing for the Ni/Ta and Fe/Ta systems, as calculated by Miedema *et al.*,[25] we found that $D_{\lambda,1}=0.995D$ for $d=100$ Å. Thus, Fickian diffusion is a good approximation for the $Ni_{81}Fe_{19}$/Ta system with multilayers of periods $d>100$ Å.

[1] B. Dieny, Europhys. Lett. **17**, 261 (1992).
[2] S. S. P. Parkin, Appl. Phys. Lett. **60**, 512 (1992).
[3] A. F. Mayadas and M. Shatzkes, Phys. Rev. B **1**, 1382 (1970).
[4] S. Krongelb, A. Gangulee, and G. Das, IEEE Trans. Magn. **9**, 568 (1973).
[5] R. L. Anderson, A. Gangulee, and L. T. Romankiw, J. Electron. Mater. **2**, 161 (1973).
[6] W. W. Mullins, J. Appl. Phys. **28**, 333 (1957).
[7] D. J. Srolovitz and C. V. Thompson, Thin Solid Films **139**, 133 (1986).
[8] L. G. Chow, S. K. Decker, D. J. Pocker, G. C. Pendley, and J. Papadopoulos, IEEE Trans. Magn. **15**, 1833 (1979).
[9] F. Spaepen, Mater. Res. Soc. Symp. Proc. **37**, 207 (1985).
[10] B. Dieny, V. S. Speriousu, B. A. Gurney, S. S. P. Parkin, D. R. Wilhoit, S. Metin, D. T. Peterson, and S. Nadimi, J. Magn. Magn. Mater. **93**, 101 (1991).
[11] P. Hansen, *Constitution of Binary Alloys* (McGraw-Hill, New York, 1958), p. 1045.
[12] R. M. Bozorth, *Ferromagnetism* (Van Nostrand, Amsterdam, 1957), p. 823.
[13] C. V. Thompson, Annu. Rev. Mater. Sci. **20**, 245 (1990).
[14] L. M. Goldman, H. A. Atwater, and F. Spaepen, Proc. Mater. Res. Soc. **160**, 571 (1990).
[15] A. M. Kadin and J. E. Keem, Scr. Metall. **20**, 443 (1986).
[16] I. Hashim and H. A. Atwater (unpublished).
[17] R. Hoffman, F. Pickus, and R. Wood, Trans. AIME **206**, 483 (1956).
[18] N. L. Peterson, in *Solid State Physics*, edited by F. Seitz, D. Turnbull, and H. Ehrenreich (Academic, New York, 1968), Vol. 22.
[19] P. G. Shewmon, *Diffusion in Solids* (Williams Book Company, Jenks, 1983), pp. 164–175.
[20] M. A. Hollanders, C. G. Duterloo, B. J. Thijsse, and E. J. Mittemeijer, J. Mater. Res. **6**, 1862 (1991).
[21] R. W. Johnson, C. C. Ahn, and E. R. Ratner, Phys. Rev. B **40**, 8139 (1989).
[22] M. Goto, H. Tange, and T. Kamimori, J. Magn. Magn. Mater. **62**, 251 (1986).
[23] J. F. Smyth, S. Schutz, D. Kern, H. Schmid, and D. Yee, J. Appl. Phys. **63**, 4237 (1988).
[24] J. W. Cahn and J. E. Hilliard, J. Chem. Phys. **28**, 258 (1958).
[25] A. R. Miedema, F. R. de Boer, and R. Boom, *CALPHAD* (Pergamon, New York, 1977), Vol. 1, pp. 341–359.